Border forces and friction control epithelial closure dynamics
Supplementary Information

Olivier Cochet-Escartin, Jonas Ranft, Pascal Silberzan and Philippe Marcq

Physico-Chimie Curie, Institut Curie,

CNRS, Université Pierre et Marie Curie,

26 rue d'Ulm, F-75248 Paris Cedex 05 France

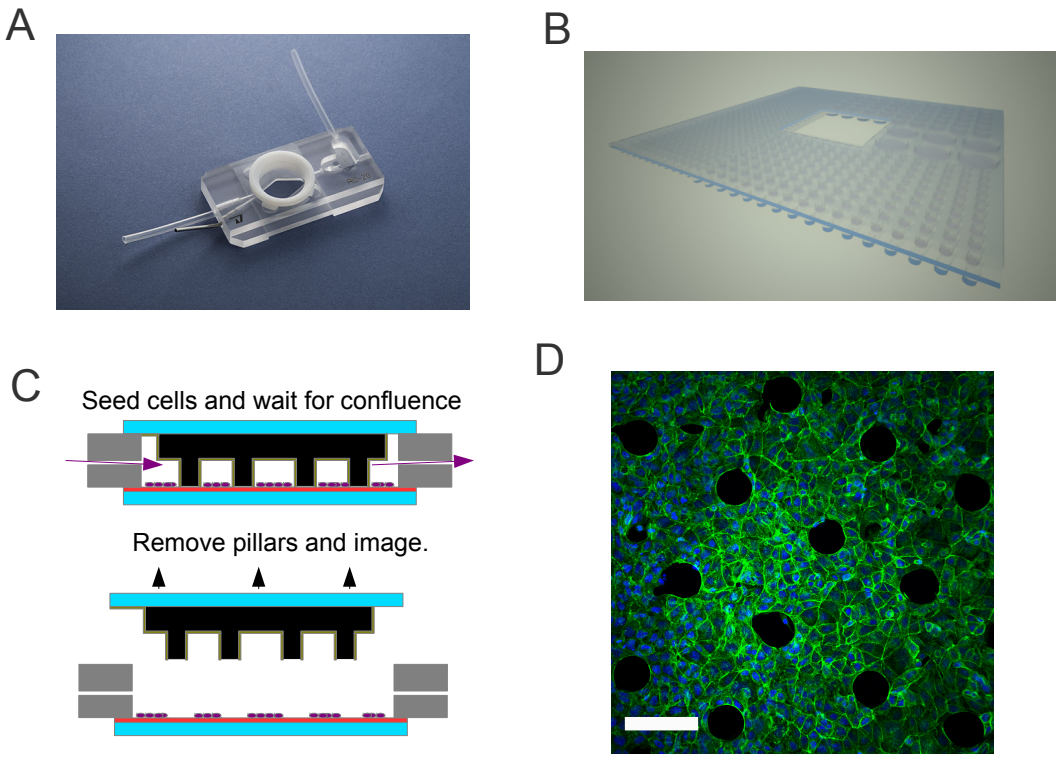

FIG. 1. **Experimental protocol and initial conditions.**

A: Picture of the flow chamber (Warner Instruments, model RC-20h).

B: Schematics of the PDMS template.

C: Schematics of the protocol. Cells are allowed to reach confluence before the template is removed.

D: MDCK wounds ($R_{\mathrm{w}} = 25\,\mu$m) were fixed while constrained under the template and labeled for F-actin (green) and nuclei (blue). Scale bar: $100\,\mu$m.

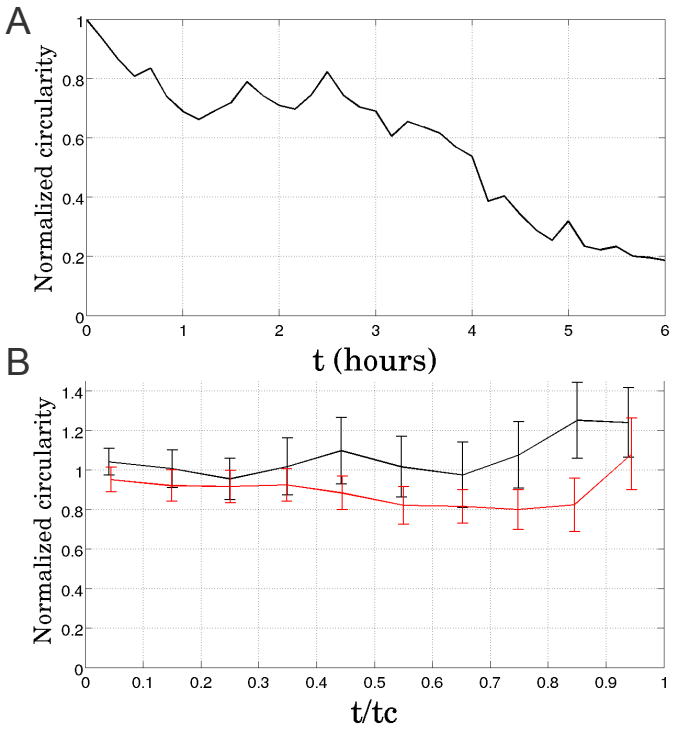

FIG. 2. **Circularity dynamics.**

A: Plot of the normalized circularity $c(t)/c(0)$ vs. time t of the large wound in Supplementary Movie 1 ($R_{\rm w} = 250\,\mu$m, red curve). The measurement stops when the fingers merge at $t = 6$h.

B: Plot of the normalized circularity $c(t)/c(0)$ vs. normalized time t/t_c, for the smallest ($R_{\rm w} = 25\,\mu$m, $N = 18$, black curve) and the largest initial radii ($R_{\rm w} = 100\,\mu$m, $N = 21$, red curve) of the small wounds. Error bars indicate the s.e.m.

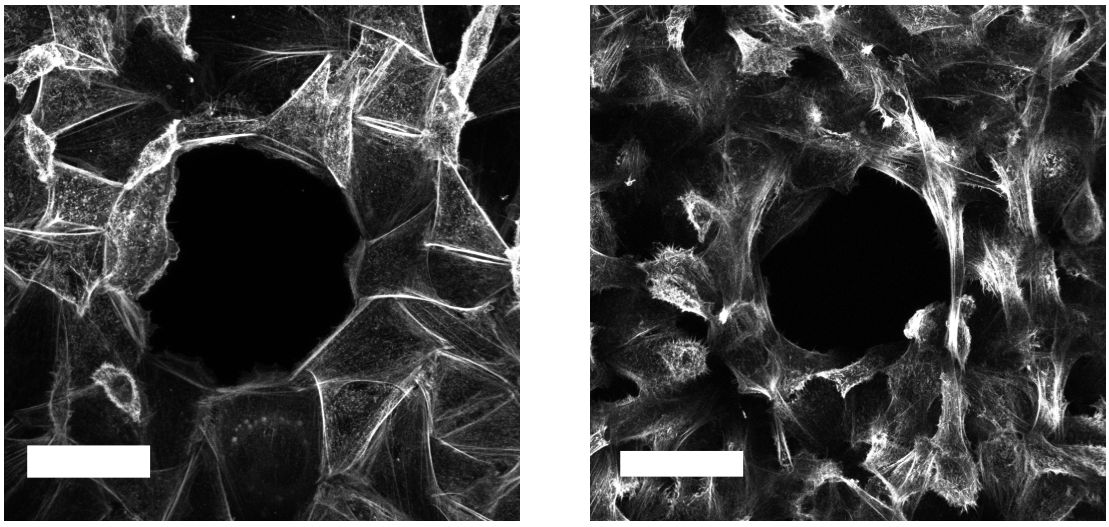

FIG. 3. **Actin staining on HEK cells.**

HEK-HT (left) and HEK-RasV12 (right) wounds ($R_{\mathrm{w}} = 50\,\mu$m) were allowed to close for 30 min and were then fixed and stained for F-actin with phalloidin. Numerous lamellipodia of different numbers and sizes are observed in both cases. Scale bar: $50\,\mu$m.

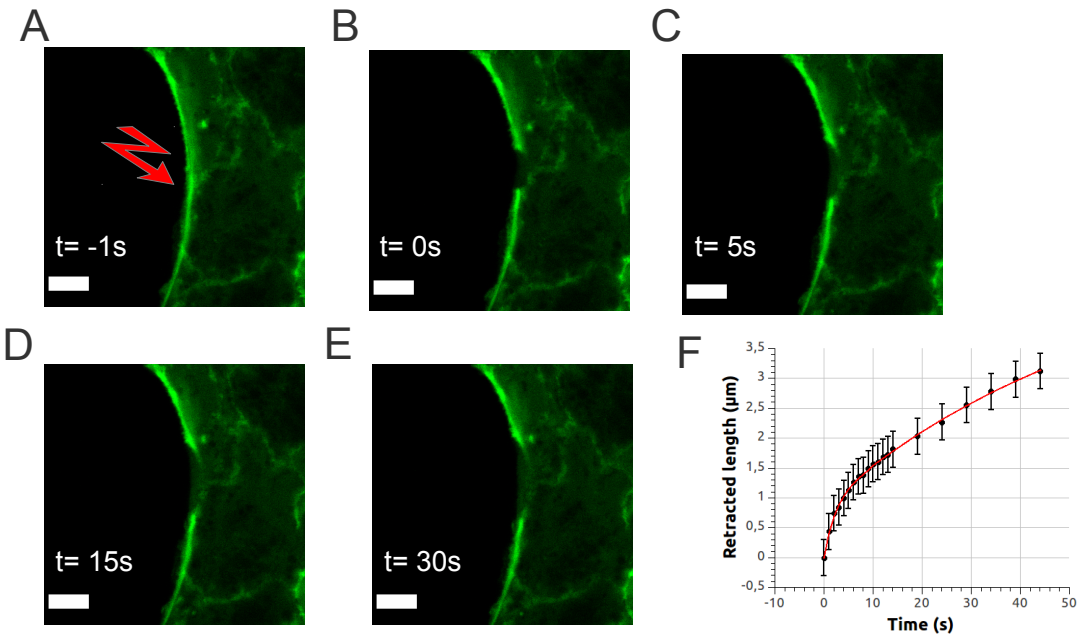

FIG. 4. **Local ablation of the acto-myosin cable.**

A-E: Timelapse of the retraction of an acto-myosin cable after laser ablation (MDCK-LifeAct-GFP wound, $R_w = 25\,\mu$m), imaged through confocal microscopy at $t = -1$ s, 0 s, 5 s, 15 s and 30 s. Here $t = 0$ s corresponds to the first image acquired immediately after ablation. Scale bar: $5\,\mu$m.

F: Retraction dynamics of one of the severed ends of the cable (black circles) with a double exponential fit (red curve) $\Delta l(t) = l_1\left(1 - e^{-t/\tau_2}\right) + l_2\left(1 - e^{-t/\tau_2}\right)$. The fit yields two characteristic times, $\tau_1 = 59.9 \pm 26.0$ s and $\tau_1 = 2.0 \pm 0.4$ s and two retraction lengths, $l_1 = 4.3 \pm 1.2\,\mu$m and $l_2 = 0.9 \pm 0.1\,\mu$m.

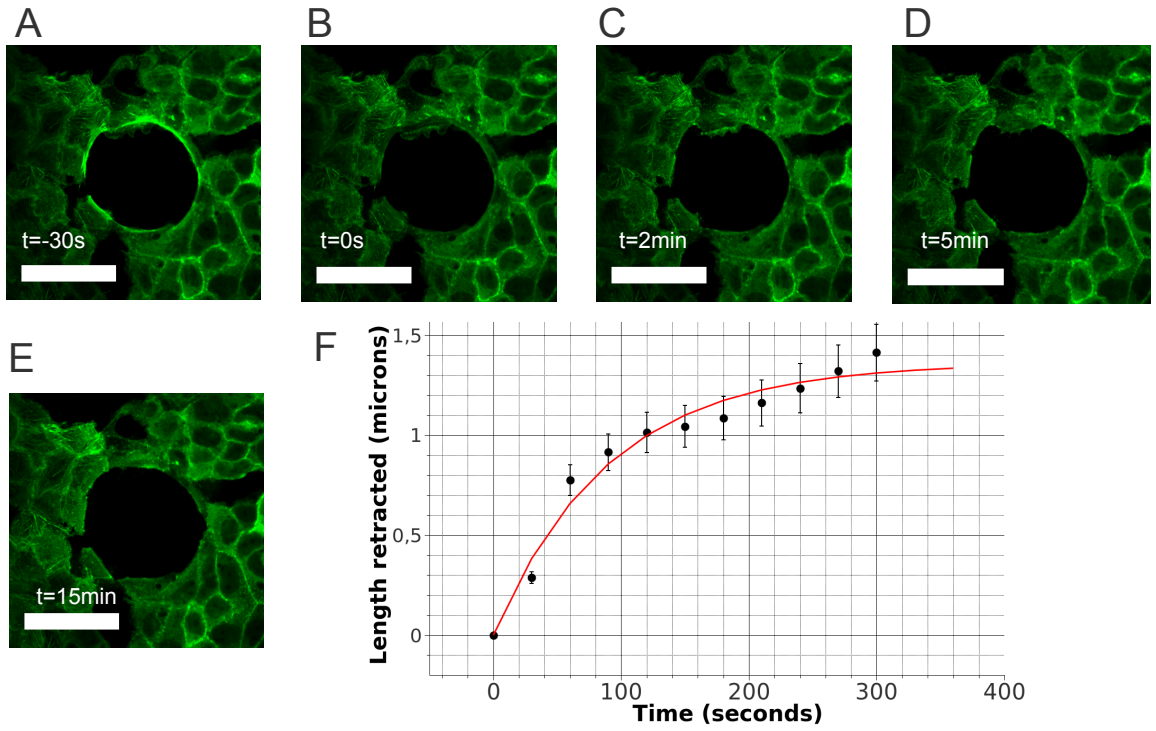

FIG. 5. **Ablation of the entire cable.**

A-E: Timelapse of the retraction of the wound edge after laser ablation of the circumferential cable (MDCK-LifeAct-GFP wound, $R_{\mathrm{w}} = 25\,\mu$m), imaged through confocal microscopy at $t = -30$ s, 0 s, 2 min, 5 min and 15 min. Here $t = 0$ s corresponds to the first image acquired immediately after ablation. Scale bar: $50\,\mu$m. The actin cable was clearly apparent before ablation.

F: Plot of the retracted wound radius as a function of time (black circles), fitted by an exponentially decaying function of time $\Delta R(t) = l\left(1 - e^{-t/\tau}\right)$ (red curve). We obtain a retracted length of $l = 1.36 \pm 0.15\,\mu$m and a retraction time of $\tau = 90.7 \pm 27.9$ s.

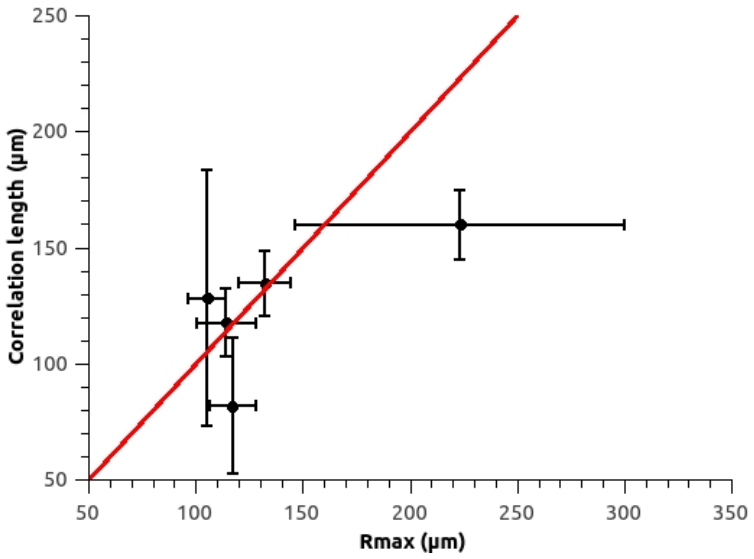

FIG. 6. **Velocity correlation length.**

Plot of the velocity correlation length vs. the cut-off radius $R_{\max}$ for all cell types and conditions. The red line is the first bissectrix, drawn to guide the eye. The cut-off radii and their error bars are obtained by fits of closure time data (see Fig. 5 and its caption). The correlation length is obtained from an exponential fit of the averaged velocity correlation function (see Methods), whose 95% confidence interval gives the error bars.

I. MODEL

We formulate a simple continuum mechanics description of wound closure, where we take advantage of our experimental observations that (i) cell division and death are negligible during the time of wound closure, (ii) there is no apparent orientational order of the cells, (iii) the wound shape remains approximately circular over the course of the experiment, and (iv) the flow is incompressible. We first detail our theoretical description (section I A), before we study three different epithelial rheologies, based on constitutive equations for either a simple inviscid or viscous liquid (sections I B and I C, respectively) or an elastic solid (section I D). Each rheology allows to obtain an analytical expression for the closure dynamics of the circular model wounds created by the experimental protocol.

A. Continuum mechanics epithelization

In order to understand wound closure dynamics on the scale of the epithelium, we aim at describing stresses and strains on large length scales, as compared to the cell size. Using continuum mechanics, we formulate an effective two-dimensional description of epithelization that takes into account the macroscopic tissue material properties.

Conservation of cell number in the epithelium is expressed by

$$\partial_t n + \partial_\alpha (n v_\alpha) = n(k_\mathrm{d} - k_\mathrm{a})\,, \tag{1}$$

where n is the cell number density, v_α the tissue velocity field, and k_d and k_a are the rates of cell division and cell death, respectively. By convention, greek indices denote vector components, and are summed when repeated. We assume $k_\mathrm{d} = k_\mathrm{a} = 0$ in the following, consistent with our experimental observations that both cell division and cell death are negligible during the time course of wound closure. Furthermore, the cell number density $n = n_0$ is approximately constant (Fig. 3E-F). The cell number balance equation then becomes a constraint on the tissue flow field, $\partial_\alpha v_\alpha = 0$: the flow is incompressible (Fig. 3B).

In a continuous material, mechanical forces are balanced locally if inertial terms can be neglected, as is the case here. Force balance is then expressed as

$$\partial_\beta \sigma_{\alpha\beta} = -f_\alpha^\mathrm{ext}\,, \tag{2}$$

where internal forces are described by the stress tensor $\sigma_{\alpha\beta}$, and $f_\alpha^{\rm ext}$ denotes external forces. Here, the external force is due to friction with the substrate, and with ξ being a friction coefficient we write $f_\alpha^{\rm ext} = -\xi v_\alpha$. Together with a constitutive equation for the stress tensor and appropriate boundary conditions, Eq. (2) allows to solve for the deformation and cell flow field in the epithelium. The constitutive equation for the stress tensor accounts for the tissue material properties. In general, the stress tensor can be decomposed into an isotropic part σ and a deviatoric (traceless) part $\tilde{\sigma}_{\alpha\beta}$ according to

$$\sigma_{\alpha\beta} = \sigma\delta_{\alpha\beta} + \tilde{\sigma}_{\alpha\beta}\,, \tag{3}$$

where $\delta_{\alpha\beta}$ denotes Kronecker's symbol, and $\tilde{\sigma}_{\alpha\alpha} = 0$ by definition.

In the following, we consider an epithelium where a model wound with initial radius R_0 is created at $t_0 = 0$, centered about the origin O. We assume that the circular shape is preserved during the closure process and denote by $R(t)$ the wound radius at time t (Fig. 4A). The wound closes because of forces exerted at the margin, either by actively pulling cells or by an acto-myosin cable that spans over the whole perimeter. Using polar coordinates, the stress boundary condition at the margin reads

$$\sigma_{rr}|_{R(t)} = \sigma_{\rm p} + \frac{\gamma}{R}\,, \tag{4}$$

where $\sigma_{\rm p}$ is a protrusive stress that accounts for forces exerted by the cells at the wound margin, and γ is a tension that describes purse-string forces due to an acto-myosin cable around the wound. Introducing the length scale $R_\gamma = \gamma/\sigma_{\rm p}$, we expect that the purse-string mechanism (resp. the protrusive forces) will dominate the dynamics at scales smaller (resp. larger) than R_γ.

Assuming rotational invariance of the flow allows to express the velocity field as $\vec{v} = v_r(r,t)\,\vec{e}_r$, where the non-vanishing radial component depends only on the distance r relative to the center O of the initial wound. Using the incompressibility constraint $\nabla\cdot\vec{v} = 0$, we obtain $v_r(r,t) = A(t)/r$, where $A(t)$ can be determined from the kinematic boundary condition at the margin. Since $v_r(r = R(t), t) = \dot{R}(t)$, we can express $v_r(r,t)$ in terms of r and the wound radius $R(t)$ only

$$v_r(r,t) = \frac{R(t)\dot{R}(t)}{r}\,. \tag{5}$$

Using this expression with Eqs. (2) and (4) allows to find a dynamical equation for the wound radius $R(t)$. In the following sections, we derive and solve this dynamical equation—

or rather the inverse problem t = t(R)—for three different constitutive equations, each highlighting a different epithelial rheology.

B. Inviscid fluid

For simplicity, we first assume that the epithelium behaves as an incompressible, inviscid fluid on the relevant time and length scales. In this case, the stresses are purely isotropic and do not depend on tissue viscosity or elasticity. In the incompressible limit, the isotropic part of the stress becomes a Lagrange multiplier which is determined from the mechanical boundary conditions, and we simply write $\sigma = -P$. The stress tensor thus reads

$$\sigma_{\alpha\beta} = -P\,\delta_{\alpha\beta}\,, \tag{6}$$

where P is the pressure field at the scale of the epithelium. Using rotational invariance ($P = P(r,t)$) and Eq. (5) for the velocity field, the force balance (2) becomes $\partial_r P = -\xi R\dot{R}/r$. The pressure follows as $P = -\xi R\dot{R}\ln r + C$, where $C = C(t)$ is a function of time. Note that in principle, $C(t)$ is determined by the boundary condition at $r \to \infty$, which is an ill-defined limit in two dimensions. We therefore introduce a constant, long-range cut-off $R_{\max}$ at which the pressure vanishes and write

$$P(r,t) = -\xi R(t)\dot{R}(t)\ln\frac{r}{R_{\max}}\,. \tag{7}$$

Since $\dot{R}(t) \le 0$ and $r \le R_{\max}$, the pressure is negative: the epithelium is under tension.

A dynamical equation for the wound radius $R(t)$ follows from the stress boundary condition at the margin, Eq. (4), and with the above expression for P we find

$$\xi R\ln\left(\frac{R}{R_{\max}}\right)\dot{R} = \sigma_{\rm p} + \frac{\gamma}{R}\,. \tag{8}$$

Using the characteristic length $R_\gamma = \gamma/\sigma_{\rm p}$, we rewrite the evolution equation as

$$\mathrm{d}t = \frac{\xi}{\sigma_{\rm p}}\,\frac{R^2}{R+R_\gamma}\ln\left(\frac{R}{R_{\max}}\right)\mathrm{d}R\,. \tag{9}$$

Integration yields the function $t(R) = \tilde{t}(R) - \tilde{t}(R_0)$, with

$$\begin{aligned} 4D\,\tilde{t}(R) = -R^2\,&\left(1 + 2\ln\frac{R_{\max}}{R}\right) \\ &+\,4R_\gamma R\left(1+\ln\frac{R_{\max}}{R}\right) + 4R_\gamma^2\left(\mathrm{Li}_2(-\frac{R}{R_\gamma}) - \ln\frac{R_{\max}}{R}\ln\frac{R+R_\gamma}{R_\gamma}\right)\,. \end{aligned} \tag{10}$$

Here, we introduce the epithelization coefficient $D = \sigma_\mathrm{p}/\xi$, which has the dimension of a diffusion coefficient, and Li_2 stands for the dilogarithm function defined as $\mathrm{Li}_2(x) = \sum_{k=1}^{\infty} x^k/k^2$. The integration constant is determined by the initial condition $t(R_0) = 0$. Since $\mathrm{Li}_2(0) = 0$, the closure time is finite: $t_\mathrm{c} \equiv t(R=0) = \tilde{t}(0) - \tilde{t}(R_0) = -\tilde{t}(R_0)$.

When the contribution of the acto-myosin cable is negligible, $R_\gamma \to 0$, the expression for $t(R)$ simplifies to

$$t(R) \simeq \frac{R_0^2}{4D}\left(1 + 2\ln\frac{R_\mathrm{max}}{R_0}\right) - \frac{R^2}{4D}\left(1 + 2\ln\frac{R_\mathrm{max}}{R}\right), \tag{11}$$

and the closure time follows as

$$t_\mathrm{c}(R_0) \simeq \frac{R_0^2}{4D}\left(1 + 2\ln\frac{R_\mathrm{max}}{R_0}\right) \tag{12}$$

in the same limit. This result implies that under the above assumptions, *i.e.*, for an inviscid epithelium, the closure of a circular model wound completes in a finite time, independently of whether a contractile cable contributes to force production or not.

C. Viscous fluid

Taking into account viscous stresses, the deviatoric stress tensor is given by

$$\tilde{\sigma}_{\alpha\beta} = 2\eta\tilde{v}_{\alpha\beta}\,, \tag{13}$$

where η is an effective tissue shear viscosity and $\tilde{v}_{\alpha\beta}$ is the traceless part of the velocity gradient tensor $v_{\alpha\beta} = \frac{1}{2}(\partial_\alpha v_\beta + \partial_\beta v_\alpha)$. The isotropic part of the stress becomes again a Lagrange multiplier, and we write $\sigma = -P$ as before. Incompressibility also implies that $v_{\gamma\gamma} = 0$, and thus $\tilde{v}_{\alpha\beta} = v_{\alpha\beta}$.

Taking into account rotational invariance, the radial component of the force balance (2) reads

$$\partial_r\sigma + \partial_r\tilde{\sigma}_{rr} + 2\frac{\tilde{\sigma}_{rr}}{r} = \xi v_r\,. \tag{14}$$

Inserting the constitutive equations, we obtain as before $\partial_r P = -\xi R\dot{R}/r$. Expression (7) for the pressure field is therefore unchanged. With $\sigma_{rr} = -P + 2\eta\,\partial_r v_r$, the boundary condition (4) now leads to

$$\dot{R} = \frac{\gamma + \sigma_\mathrm{p} R}{\xi R^2 \ln R/R_\mathrm{max} - 2\eta}\,. \tag{15}$$

Introducing the length scale $R_\eta = \sqrt{\eta/\xi}$, integration yields

$$t(R) = \tilde{t}(R) - \tilde{t}(R_0)\,, \tag{16}$$

with

$$\begin{aligned} 4D\,\tilde{t}(R) = &-R^2\left(1 + 2\ln\frac{R_{\max}}{R}\right) + 8R_\eta^2\,\ln\frac{R_{\max}}{R+R_\gamma} \\ &+ 4R_\gamma R\left(1 + \ln\frac{R_{\max}}{R}\right) + 4R_\gamma^2\left(\mathrm{Li}_2(-\frac{R}{R_\gamma}) - \ln\frac{R_{\max}}{R}\ln\frac{R+R_\gamma}{R_\gamma}\right)\,. \end{aligned} \tag{17}$$

In the limit of vanishing viscosity, $R_\eta \to 0$, the above expression reduces to Eq. (10), consistent with the assumption of vanishing deviatoric stresses in the inviscid case.

The closure time is again finite, $t_\mathrm{c} \equiv t(R=0) = \tilde{t}(0) - \tilde{t}(R_0) = 2(\eta/\sigma_\mathrm{p})\,\ln(R_{\max}/R_\gamma) - \tilde{t}(R_0)$, and tends to expression (12) in the limit where both R_η and R_γ are negligible. However, if R_η remains finite, the closure time diverges in the limit $R_\gamma \to 0$. The model predicts that, in the absence of a contractile cable, circular model wounds do not complete closure in finite time when viscous stresses in the epithelium cannot be neglected. This somewhat surprising result is an artifact of the continuous description: in fact closure will complete, thanks to cell-scale mechanisms not taken into account by the model, as soon the wound radius is smaller than a microscopic cut-off length a, with a finite closure time of the order of $\tilde{t}(a) - \tilde{t}(R_0)$.

D. Elastic solid

When deformations are small, the constitutive equation for an incompressible elastic material reads

$$\tilde{\sigma}_{\alpha\beta} = 2\mu\tilde{u}_{\alpha\beta}\,, \tag{18}$$

where μ is the shear elastic modulus and $\tilde{u}_{\alpha\beta}$ is the traceless part of the strain tensor. The latter is defined as $u_{\alpha\beta} = \frac{1}{2}(\partial_\alpha u_\beta + \partial_\beta u_\alpha)$ for a displacement field u_α. Incompressibility implies that $u_{\gamma\gamma} = 0$, and thus $\tilde{u}_{\alpha\beta} = u_{\alpha\beta}$. In this limit, the isotropic stress becomes again a Lagrange multiplier and we write $\sigma = -P$.

In the case of rotational invariance, we can express the elastic displacement field as $\vec{u} = u_r(r,t)\,\vec{e}_r$. Using the incompressibility condition $\nabla\cdot\vec{u} = 0$ together with the boundary condition $u_r(R,t) = R(t) - R_0$, we obtain u_r as a function of r and $R(t)$,

$$u_r(r,t) = \frac{R(t)(R(t)-R_0)}{r}\,. \tag{19}$$

One can check that this expression verifies $\dot{R}(t) \equiv (\partial_t + v_r\partial_r)\, u_r(r = R(t), t) = v_r(r = R(t), t)$ at all times $t \geq 0$. The differential equation for P resulting from force balance is again unchanged, P is given by Eq. (7). Since the radial stress in the epithelium is given by

$$\sigma_{rr} = -P + 2\mu\partial_r u_r\,, \tag{20}$$

the stress boundary condition (4) yields the following dynamical equation for the wound radius $R(t)$

$$\dot{R} = \frac{\gamma + \sigma_{\rm p} R + 2\mu(R - R_0)}{\xi R^2 \ln R/R_{\rm max}}\,. \tag{21}$$

Formally, elastic restoring forces and forces driving epithelization balance at the equilibrium radius $R_{\rm e}$ with

$$R_{\rm e} = \frac{2\mu R_0 - \gamma}{\sigma_{\rm p} + 2\mu}\,. \tag{22}$$

Taking into account the initial condition $t(R_0) = 0$, integration of Eq. (21) yields

$$t(R) = \tilde{t}(R) - \tilde{t}(R_0)\,, \tag{23}$$

where $\tilde{t}(R)$ is given by

$$4D_S\,\tilde{t}(R) = -R^2 - 4RR_{\rm e} + 2R\,(R + 2R_{\rm e})\ln\frac{R}{R_{\rm max}} + 4R_{\rm e}^2\left(\ln\frac{R}{R_{\rm max}}\ln\left(1 - \frac{R}{R_{\rm e}}\right) + {\rm Li}_2\left(\frac{R}{R_{\rm e}}\right)\right)\,. \tag{24}$$

Here, $D_{\rm S} = \frac{\sigma_{\rm p}+2\mu}{\xi}$ has the dimension of a diffusion coefficient, and differs from the epithelization coefficient D by a factor of $(1 + \frac{2\mu}{\sigma_{\rm p}})$. In the limit of vanishing elastic modulus ($2\mu \ll \sigma_{\rm p}$ and $2\mu \ll \gamma/R_0$), expression (24) for $t(R)$ reduces to the one obtained for an inviscid fluid as given by Eq. (10). Of course only positive values of the radius are physical and closure stops when $R(t_c) = 0$.

The above result for $t(R)$ implies that the wound closure eventually completes whenever $R_{\rm e} \leq 0$. This is the case for large enough values of the line tension γ, *i.e.*, $\gamma \geq 2\mu R_0$. The closure time is then given by $t_{\rm c} = t(R = 0) = \tilde{t}(0) - \tilde{t}(R_0) = -\tilde{t}(R_0)$. In the particular case where line tension and elasticity balance exactly, $\gamma = 2\mu R_0$ and thus $R_{\rm e} = 0$, Eq. (24) reduces to Eq. (11), and the closure time follows as given by Eq. (12) with the substitution $D \to D_S$.

When the equilibrium radius is positive but small, $0 < R_{\rm e} \simeq a$, where a is of the order of the size of a cell, epithelization may proceed to a scale small enough that microscopic

mechanisms, not accounted for within the continuous description, terminate the epithelization process. This might be the case even for small values of the line tension $0 \leq \gamma \leq 2\mu R_0$ provided that the protrusive stress dominates the elastic modulus, $\sigma_\mathrm{p} \gg 2\mu$ (see Eq. (22)).

When the epithelial elastic modulus is large enough ($2\mu \sim \sigma_\mathrm{p}$ and $2\mu > \gamma/R_0$), the equilibrium radius is strictly positive: wound closure halts due to elastic forces. Expression (24) takes complex values when $R_\mathrm{e} > 0$. However, the identity

$$\mathrm{Li}_2(x) + \mathrm{Li}_2(1-x) + \ln(1-x)\ln x = \frac{\pi^2}{6} \tag{25}$$

allows to rewrite $t(R)$ as

$$t(R) = \frac{\xi}{4\,(\sigma_\mathrm{p}+2\mu)}\left[(R_0^2-R^2) + 4(R_0-R)R_\mathrm{e} + 2R\,(R+2R_\mathrm{e})\ln\frac{R}{R_\mathrm{max}}\right.$$
$$\left. - 2R_0\,(R_0+2R_\mathrm{e})\ln\frac{R_0}{R_\mathrm{max}} + 4R_\mathrm{e}^2\left(\mathrm{Li}_2(1-\frac{R_0}{R_\mathrm{e}}) - \mathrm{Li}_2(1-\frac{R}{R_\mathrm{e}}) + \ln\frac{R-R_\mathrm{e}}{R_0-R_\mathrm{e}}\ln\frac{R_\mathrm{e}}{R_\mathrm{max}}\right)\right], \tag{26}$$

where all terms are real-valued for $R > R_\mathrm{e} > 0$. In this case the closure time is infinite.

II. DATA ANALYSIS

In section I, we obtained analytical expressions of $t_\mathrm{c}(R_0)$ and $t(R)$, corresponding to different epithelial rheologies. In order to estimate the physical parameters of the epithelia, we now fit experimental data by these expressions, using the Levenberg-Marquardt algorithm for nonlinear least-squares fitting, implemented in PYTHON (LMFIT package, `http://pypi.python.org/pypi/lmfit/`, Least-Squares Minimization with Bounds and Constraints). We successively examine fits of closure times vs. initial effective radii in section II A and fits of individual trajectories $R(t)$ in section II B.

A. Closure time data

The closure time is a robust quantity that depends only weakly on the image analysis method: at a given time t, the wound is either open or closed. The experimental uncertainty on t_c is of the order of the time resolution of data acquisition, between 3 and 15 minutes depending on the size of the wound. Fig. 7 gives the empirical cumulative distribution functions of closure times for MDCK wounds, including the effect of inhibitors. Fig. 8

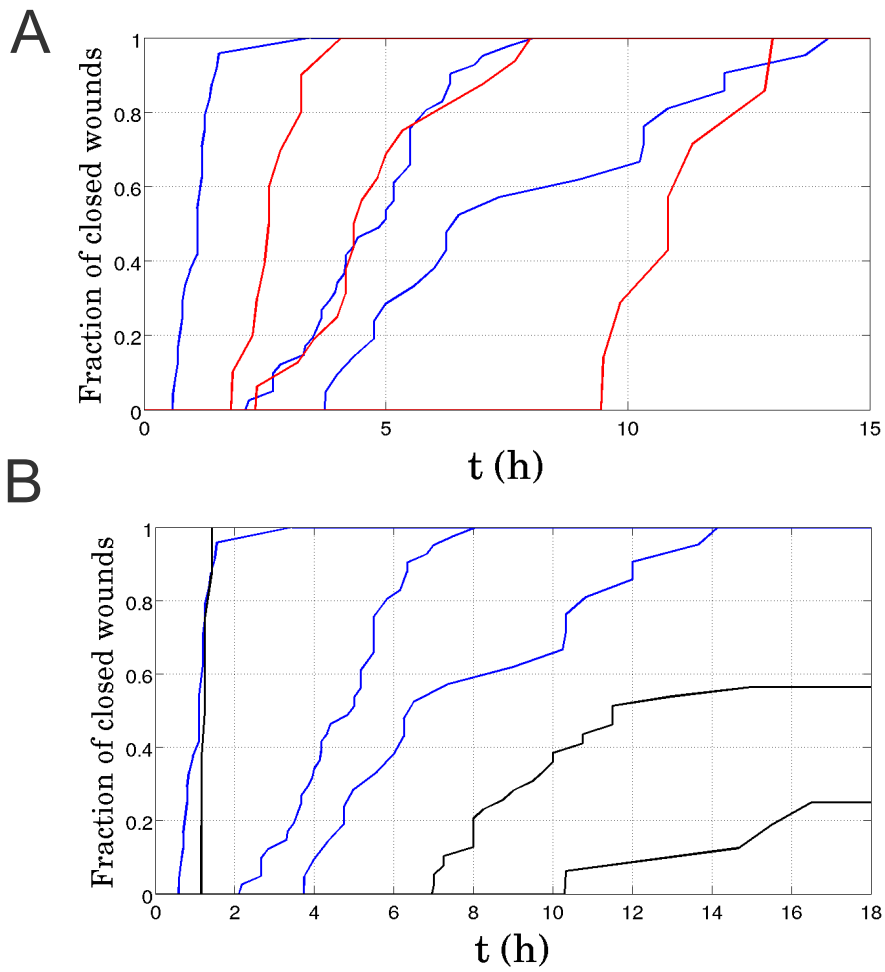

FIG. 7. **Cumulative distributions of closure times for MDCK wounds.**

A: comparison between wild-type (blue curves, $N = 24$, 41 and 16 respectively) and Rho$^-$ assays (red curves, $N = 10$, 16 and 7 respectively), $R_\mathrm{w} = 25\,\mu$m, $50\,\mu$m and $100\,\mu$m from left to right.

B: comparison between wild-type (blue curves, same data as in A) and Rac$^-$ assays (red curves, $N = 8$, 39 and 16 respectively), same sizes from left to right. A fraction of the Rac$^-$ wounds do not complete closure within the observation time $t = 18$ h.

shows that closure time data pertaining to all cell types and conditions is well fitted by Equation (12), obtained for an inviscid epithelium without cable.

We now ask whether this simple description is robust, and consider this question in the case of MDCK wild-type wounds, for which the number of wounds is largest ($N = 130$). As shown in section I, different assumptions made on the epithelial rheology lead to different expressions of the closure time t_c as a function of the initial radius R_0. Although an

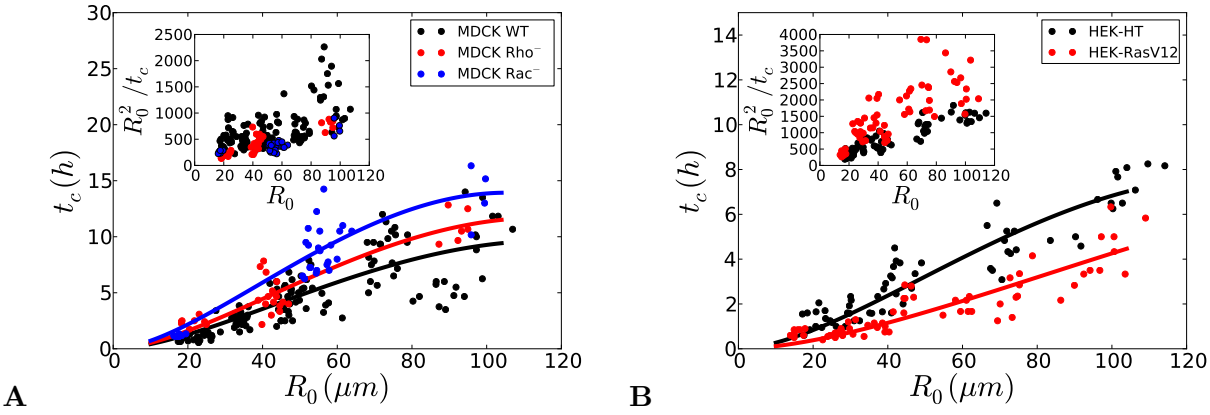

FIG. 8. **Inviscid fluid:** Closure time t_c as a function of the initial effective radius R_0 (circles), fitted by Equation (27) (solid curves) with the constraints $D, R_{\max} \geq 0$. One dot corresponds to one wound.

A: MDCK wounds. Wild Type, Rho$^-$ and Rac$^-$ assays. The physical parameters of epithelization $(D, R_{\max})$ are given within a 95 % confidence interval. MDCK WT ($N = 130$): $\sigma_p/\xi = 353 \pm 38\,\mu m^2\,h^{-1}$, $R_{\max} = 117 \pm 11\,\mu m$; MDCK Rho$^-$ ($N = 30$): $\sigma_p/\xi = 278 \pm 40\,\mu m^2\,h^{-1}$, $R_{\max} = 114 \pm 14\,\mu m$; MDCK Rac$^-$ ($N = 34$): $\sigma_p/\xi = 198 \pm 22\,\mu m^2\,h^{-1}$, $R_{\max} = 105 \pm 9\,\mu m$;

B: HEK-HT and HEK-RasV12 wounds. HEK-HT ($N = 63$): $\sigma_p/\xi = 572 \pm 57\,\mu m^2\,h^{-1}$, $R_{\max} = 132 \pm 12\,\mu m$; HEK-RasV12 ($N = 65$): $\sigma_p/\xi = 1531 \pm 363\,\mu m^2\,h^{-1}$, $R_{\max} = 223 \pm 77\,\mu m$.

Insets: for all cell types and conditions, the ratio of initial effective area over closure time R_0^2/t_c increases with initial radius R_0.

inviscid epithelium may close without cable, strictly speaking, both a viscous and an elastic epithelium require a finite line tension ($\gamma \neq 0$) for closure to reach completion.

For convenience, we summarize below the analytical expressions obtained for $t_c(R_0)$:

- *inviscid liquid, without cable* ($\gamma = 0$, $D = \sigma_p/\xi$):

$$4D\,t_c(R_0) = R_0^2\left(1 + 2\ln\frac{R_{\max}}{R_0}\right) \tag{27}$$

- *inviscid liquid, with cable* ($\gamma \neq 0$, $R_\gamma = \gamma/\sigma_p$):

$$4D\,t_c(R_0) = R_0^2\left(1 + 2\ln\frac{R_{\max}}{R_0}\right) - 4R_0R_\gamma\left(1 + \ln\frac{R_{\max}}{R_0}\right) - 4R_\gamma^2\left(\mathrm{Li}_2(-\frac{R_0}{R_\gamma}) + \ln\frac{R_{\max}}{R_0}\ln\frac{R_\gamma}{R_0 + R_\gamma}\right) \tag{28}$$

- *viscous liquid, with cable* ($R_\eta = \sqrt{\eta/\xi}$):

$$4D\,t_{\rm c}(R_0) = R_0^2\left(1+2\ln\frac{R_{\rm max}}{R_0}\right) - 4R_0R_\gamma\left(1+\ln\frac{R_{\rm max}}{R_0}\right) + 8R_\eta^2\,\ln\frac{R+R_\gamma}{R_\gamma} - 4R_\gamma^2\left(\mathrm{Li}_2(-\frac{R_0}{R_\gamma}) + \ln\frac{R_{\rm max}}{R_0}\ln\frac{R_\gamma}{R_0+R_\gamma}\right) \quad (29)$$

- *elastic solid, with cable* ($R_{\rm e} = \frac{2\mu R_0-\gamma}{\sigma_{\rm p}+2\mu} \leq 0$, $D_S = \frac{\sigma_{\rm p}+2\mu}{\xi}$):

$$4D_S\,t_{\rm c}(R_0) = R_0^2\left(1+2\ln\frac{R_{\rm max}}{R_0}\right) + 4R_0R_{\rm e}\left(1+\ln\frac{R_{\rm max}}{R_0}\right) - 4R_{\rm e}^2\left(\mathrm{Li}_2(\frac{R_0}{R_{\rm e}}) - \ln\frac{R_{\rm max}}{R_0}\ln(1-\frac{R_0}{R_{\rm e}})\right) \quad (30)$$

First, we investigate whether cable tension may significantly contribute to force production at the margin (Fig. 9A). Fitting closure time data with expression (28), obtained for an inviscid epithelium with a cable, we find that:

- values of D and $R_{\rm max}$ are consistent within error bars with those obtained without a cable;

- the length scale $R_\gamma = 7 \pm 11\,\mu$m is small compared to R_0 ($R_\gamma \ll R_0$), as well as to the wound radius ($R_\gamma \ll R(t)$) except in the late stages of closure.

When the epithelium is modeled as an inviscid fluid, we conclude that the contribution of the actomyosin cable to the stress boundary condition is negligible. For the sake of completeness, we investigate the case where protrusive forces are small compared to the cable tension ($R_\gamma \gg R_0$). In this case, the closure time is given by

$$9\frac{\gamma}{\xi}\,t_{\rm c}(R_0) = R_0^3\left(1+3\ln\frac{R_{\rm max}}{R_0}\right), \quad (31)$$

which follows from integration of Eq. (8) with $\sigma_{\rm p} = 0$. This expression fits the closure time data rather poorly (Fig. 9A): in particular the value obtained for $R_{\rm max}$ is inconsistent with the sizes considered. We conclude that protrusive forces at the margin cannot be neglected.

Second, we ask whether neglecting viscous stresses in the epithelium is legitimate, and fit data with Eq. (29) (see Fig. 9B). We obtain:

- values of D and $R_{\rm max}$ consistent within error bars with those found in the inviscid case without a cable;

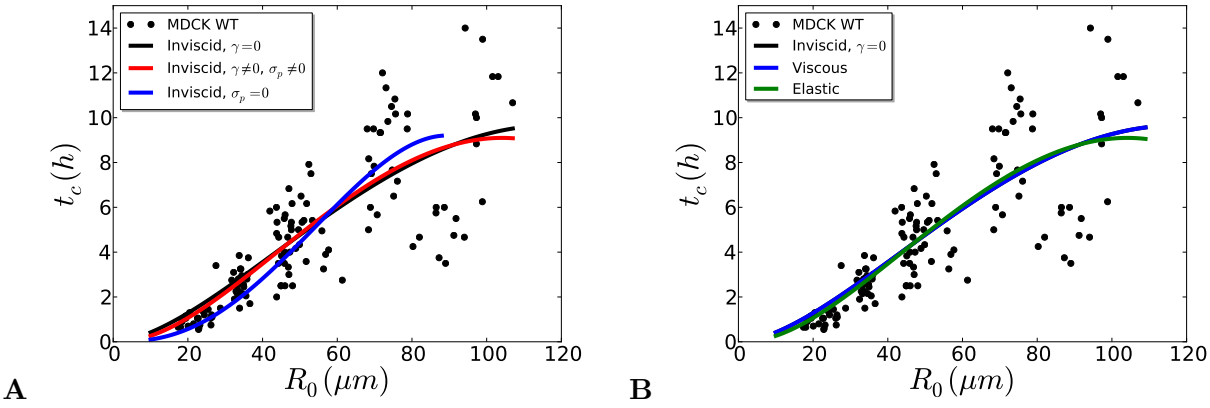

FIG. 9. **Model selection:** MDCK wild type wounds.

A Border forces. The closure time t_c is plotted as a function of the initial effective radius R_0 (black circles), and fitted by analytical expressions obtained when the epithelium is modeled as an inviscid fluid:

- Equation (27): black line, $\sigma_p \neq 0, \gamma = 0$, constraints $D, R_{max} \geq 0$, fitted parameter values $\sigma_p/\xi = 353 \pm 38\,\mu m^2\,h^{-1}$, $R_{max} = 117 \pm 11\,\mu m$;

- Equation (28): red line, $\sigma_p \neq 0, \gamma \neq 0$, constraints $D, R_{max}, R_\gamma \geq 0$, fitted parameter values $\sigma_p/\xi = 247 \pm 108\,\mu m^2\,h^{-1}$, $R_{max} = 104 \pm 13\,\mu m$, $R_\gamma = 7 \pm 11\,\mu m$;

- Equation (31): blue line , $\sigma_p = 0, \gamma \neq 0$, constraints $\gamma/\xi, R_{max} \geq 0$, fitted parameter values $\gamma/\xi = 8592 \pm 606\,\mu m^3\,h^{-1}$, $R_{max} = 89 \pm 2\,\mu m$.

B Tissue rheology. The closure time t_c is plotted as a function of the initial effective radius R_0 (black circles), and fitted by analytical expressions obtained when both lamellipodial protrusions and an actomyosin cable are taken into account ($\sigma_p \neq 0, \gamma \neq 0$):

- Equation (27): black line, inviscid fluid as in A;

- Equation (29): blue line, viscous fluid, constraints $D, R_{max}, R_\gamma, R_\eta \geq 0$, the (blue) fitted curve cannot be distinguished from the black curve, with identical parameter values of D and R_{max}, and $R_\gamma = R_\eta = 0$.

- Equation (30): green line, elastic solid, constraints $D, R_{max}, \mu, \gamma \geq 0$, the fit yields $\sigma_p/\xi \approx 247\,\mu m^2\,h^{-1}$, $R_{max} = 104\,\mu m$, $\frac{2\mu}{\sigma_p} = 0$, $R_\gamma \approx 7\,\mu m$, from which we deduce $R_e = -R_\gamma < 0$.

  - a length scale $R_\gamma = 7 \pm 51\,\mu m$, consistent with a zero value;

  - a viscous length scale $R_\eta = 0.01 \pm 8000\,\mu m$, consistent with a zero value.

We conclude that the actomyosin cable can be neglected in this case as well ($R_\gamma \ll R_0$), and that dissipation is dominated by friction with the substrate ($R_\eta \ll R_0$): epithelial viscosity can be neglected.

Finally, we study closure time data taking into account elastic stresses, and fit data with Equation (30), constraining the parameters D_s, $R_{\max}$, $2\mu/\sigma_{\mathrm{p}}$, and R_γ to be positive. The fitted value of $2\mu/\sigma_{\mathrm{p}}$ is consistent with zero: elastic forces are vanishingly small when compared to protrusive forces. In addition, the fitted values of $D_s = D$, $R_{\max}$ and R_γ are consistent with those obtained for an inviscid fluid when the cable line tension is taken into account. In this case, Equation (30) reduces to Equation (28).

Altogether, we find that the model of the monolayer as an inviscid fluid describes wild-type MDCK data satisfactorily, and that viscous and elastic contributions to the stress are negligibly small. Furthermore, the contribution of the cable to force production is small compared to that of lamellipodia. We hypothesize that the main function of the contractile circumferential cable is to stabilize the free epithelial boundary. Since $R_\gamma \ll R_0$ in all cases considered, we neglect cable tension in the following and set $\gamma = 0$ unless explicitly specified otherwise.

B. Closure trajectories

In sections II B 1 and II B 2, we examine the individual trajectories of closing and non-closing wounds.

1. Closing wounds

For brevity, we focus on MDCK-WT and HEK-HT wounds, and fit Equation (11) to data, using for convenience time as a function of radius $t(R)$. In Section II A, we showed that the simplest model of the monolayer as an inviscid fluid driven by cell protrusions at the margin suffices to describe closure time data. We therefore fit trajectories using the same model (see Fig. 10A), obtain one set of physical parameters per wound, and check the consistency of our results.

Since $R_{\max}$ was previously found to vary little, we constrain $R_{\max}$ to belong to the 95% confidence interval obtained from closure time data (see the caption of Fig. 8 for numerical

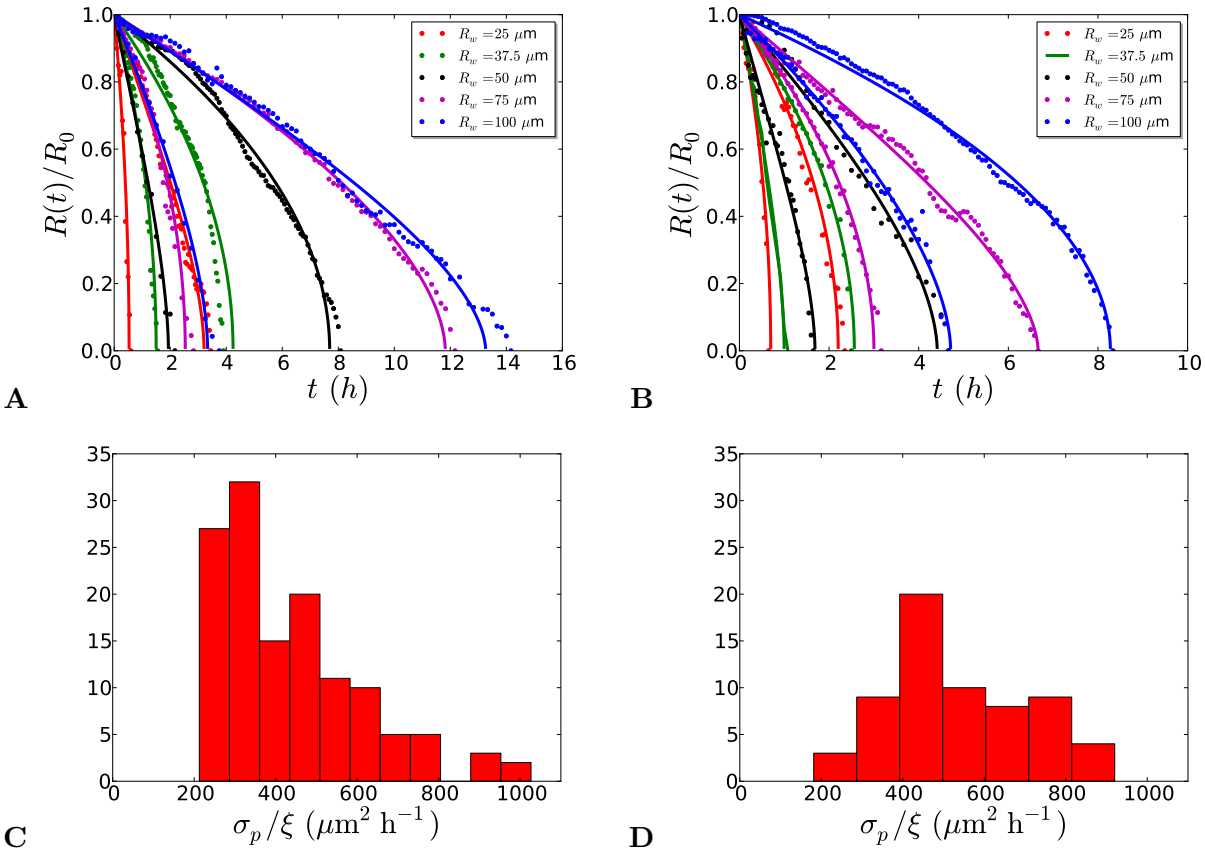

FIG. 10. **Trajectories $R(t)$ of closing wounds. A, C:** MDCK wild type wounds; **B, D:** HEK-HT wounds.

A, B: Fit of trajectories $R(t)$ with Equation (11). For clarity, we show only two trajectories (circles) and their fits (solid curves) per pillar size R_{w}, corresponding to the shortest and longest closure time observed at a given R_{w}. The normalized effective radius $R(t)/R_0$ is plotted as a function of time t.

C, D: Histogram of estimates of the epithelization coefficient (see text for details).

values). The distributions of epithelization coefficients obtained by fitting Equation (11) to data are shown in Fig. 10, for MDCK-WT and HEK-HT wounds, with mean values ± standard deviations given by:

- MDCK wild type wounds: $\sigma_{\mathrm{p}}/\xi = 424 \pm 170\,\mu\mathrm{m}^2\,\mathrm{h}^{-1}$;
- HEK-HT wounds: $\sigma_{\mathrm{p}}/\xi = 522 \pm 165\,\mu\mathrm{m}^2\,\mathrm{h}^{-1}$.

For both cell types, the confidence intervals obtained from fitting closure time data belong to the above intervals: the two measurement methods are consistent. Trajectories are noisy, due to intrinsic variabity, but also to possible pixelization errors when determining the area of the cell-free domain. Fitting individual trajectories leads to a higher dispersion of estimated parameter values. We therefore prefer to use closure time data for parameter estimation whenever closure is complete.

2. Non-closing wounds

We finally turn to the non-closing wounds observed in MDCK Rac$^-$ assays. Among the models presented in Section I, the only case where the final radius is strictly positive is that of an elastic epithelium with $R_\mathrm{e} > 0$, or $2\mu > \gamma/R_0$. In Fig. 11A, we show that individual trajectories are fitted satisfactorily by Equation (26). The equilibrium radius R_e increases with the initial effective radius R_0 (Fig. 11B), as predicted by Equation (22). A linear regression of R_e vs. R_0 yields the estimates

$$\frac{2\mu}{2\mu+\sigma_\mathrm{p}} = 0.5 \pm 0.1 \tag{32}$$

$$\frac{\gamma}{2\mu+\sigma_\mathrm{p}} = 6 \pm 7\ \mu\mathrm{m}. \tag{33}$$

From (32), we deduce that $\mu/\sigma_\mathrm{p} \approx 0.5$. Assuming that the Rac pathway has a limited influence on the epithelial elasticity, this suggests that Rac inhibition leads to lower values of the protrusive stress (compared to wild type assays), of the order of the elastic modulus. Since $\mu/\sigma_\mathrm{p} \approx 0.5$, Equation (33) yields $R_\gamma \approx 10\,\mu$m: the actomyosin cable contributes significantly to force production in non-closing Rac$^-$ assays when, *e.g.*, $R_\mathrm{w} = 50\,\mu$m.

Fitting non-closing trajectories, we obtain estimates of the coefficient $D_s = D\left(1+\frac{2\mu}{\sigma_\mathrm{p}}\right)$. Using $\mu/\sigma_\mathrm{p} \approx 0.5$, we expect that $D \approx 0.5\,D_s$. In Fig. 11C, we plot the histogram of epithelization coefficients defined for simplicity as $D = 0.5\,D_s$. We find $\sigma_\mathrm{p}/\xi = 180 \pm 45\,\mu\mathrm{m}^2\,\mathrm{h}^{-1}$ (mean value $\pm$ standard deviation, $N = 29$). Fitting Rac$^-$ closing trajectories with Equation (11) for an inviscid epithelium, we obtain $\sigma_\mathrm{p}/\xi = 230 \pm 66\,\mu\mathrm{m}^2\,\mathrm{h}^{-1}$ ($N = 30$), a value slightly higher than the previous estimate obtained for non-closing wounds. Note that both estimates are consistent with that obtained from fitting time closure data.

A balance between driving forces at the margin and a bulk elastic restoring force explains the positive value of the equilibrium radius observed in these assays. A word of caution

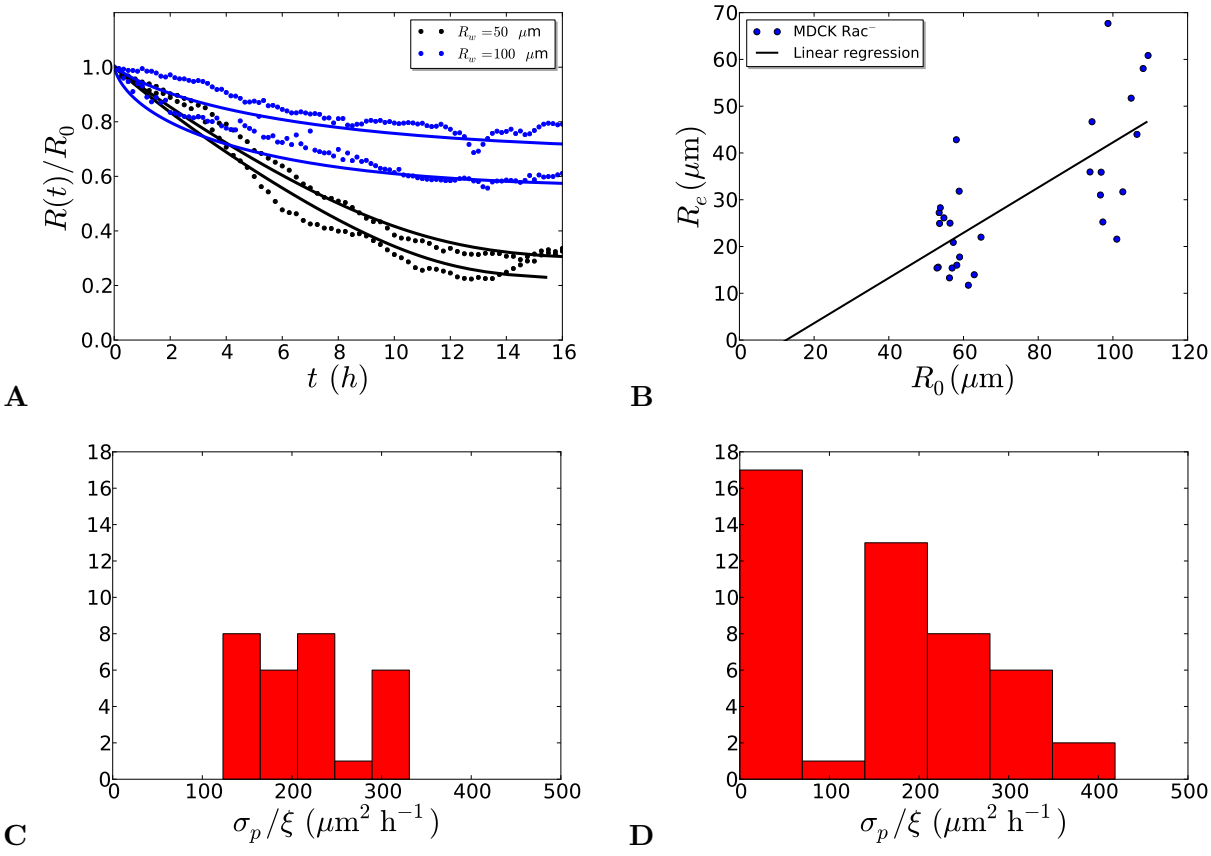

FIG. 11. **MDCK Rac$^-$ assay**

A-C: Non-closing wounds

A: Trajectories. Normalized effective radius $R(t)/R_0$ as a function of time t. For illustrative purposes, we show only two trajectories $t(R)$ per pillar size R_w (solid curves) and their fit by Equation (26) (dashed curves), with the constraints $D_S \geq 0$, $R_\mathrm{max} \in [96\ 114]\,\mu$m (confidence interval obtained from closure time data), $R_\mathrm{e} = \min R(t)$ (Equation (26) is defined only for $R > R_\mathrm{e}$).

B: Equilibrium Radius R_e (estimated as $R_\mathrm{e} = \min R(t)$) vs. initial radius R_0. The linear regression line (black solid line, $R_\mathrm{e} = aR_0 + b$) has coefficients $a = 0.5 \pm 0.1$, $b = -6 \pm 7\,\mu$m.

C: Histogram of parameter estimates. The epithelization coefficient is estimated as $D = D_s/2$ (from $2\mu/\sigma_\mathrm{p} \approx 1$), where D_s is obtained by nonlinear curve fitting of the trajectory, as in (a).

D: Closing wounds. Histogram of the epithelization coefficient. Closing trajectories are fitted as in Fig. 10A-B.

seems however in order. Although $R(t)$ plateaus on a time scale of the order of 15 h, one cannot exclude that a "non-closing wound" may in fact heal completely on a time scale much

longer than the available observation time, over which cell divisions may become relevant and need to be taken into account.

MOVIE 1. **Closure of a large MDCK circular wound.**
A MDCK-actin-GFP wound ($R_w = 250\,\mu$m) is imaged in epifluorescence for 14 h. Scale bar: $200\,\mu$m. Three leader cells formed at the edge of the wound and then drove multicellular fingers hence deforming the initial circle (Fig. 6). The fingers eventually met in the center and the leader cells switched back to a classical epithelial phenotype. The remaining secondary wounds then proceeded to heal in a much more regular fashion without showing any formation of leader cells (Movie 2).

MOVIE 2. **Closure of "secondary" wounds.**
Close-up on the secondary wounds from the experiment seen in Movie 1, imaged for 8.3 h. Scale bar: $100\,\mu$m. Neither leader cells and nor margin roughening are seen.

MOVIES 3-5. **Closure of small circular wounds.**
Three examples of time lapse movies made in phase contrast microscopy showing the typical closure of a wound for, respectively:

- wild type MDCK cells, $R_w = 50\,\mu$m for 6 h 30; scale bar: $100\,\mu$m;
- HEK-HT cells, $R_w = 50\,\mu$m for 4 h; scale bar: $100\,\mu$m;
- HEK-RasV12 cells, $R_w = 75\,\mu$m for 3 h 30; scale bar: $150\,\mu$m.

Direct inspection shows that the protrusive activity is enhanced in the last case, with a closure time shorter compared to a smaller wild type HEK wound.

MOVIE 6. **Dynamics of lamellipodial activity.**
A MDCK-LifeAct-GFP wound ($R_w = 25\,\mu$m) was imaged by confocal microscopy for 3 h. Scale bar: $25\,\mu$m. The optical slice was very close to the surface as this is the position where lamellipodia develop. For this reason, stress fibers were apparent but the membranes between cells were not. We observed a high number and a large activity of these lamellipodia that could be recognized as waves of actin in the bulk of the tissue. Of note, high laser power was needed to observe these lamellipodia and the dynamics of closure was drastically reduced in those experiments probably due to phototoxicity.

MOVIE 7. **Laser ablation of the entire cable.**
A MDCK LifeAct-GFP wound ($R_w = 25\,\mu$m) is imaged by confocal microscopy from $t = 30$

min after removal of the pillars. The actin cable is then fully ablated and the retraction of the edge is imaged for 1 min. Note the dynamic retraction of the edge of the wound. Scale bar : $10\,\mu$m.

MOVIE 8. **A non closing MDCK Rac$^-$ wound.**
A MDCK wound ($R_\mathrm{w} = 50\,\mu$m) under Rac inhibition was imaged in phase contrast. The movie runs for 17.5 h. Scale bar: $100\,\mu$m.